JGR Oceans

RESEARCH ARTICLE
10.1029/2022JC018833

Key Points:

- Water mass mixing and biogeochemical activity are the major drivers of seasonal carbonate system dynamics in the Mid-Atlantic Bight
- Water mass mixing has opposing effects on carbonate chemistry in the nearshore and at the continental shelf break

Supporting Information:

Supporting Information may be found in the online version of this article.

Correspondence to:

E. K. Wright-Fairbanks,
liza.wright-fairbanks@noaa.gov

Citation:

Wright-Fairbanks, E. K., & Saba, G. K. (2022). Quantification of the dominant drivers of acidification in the coastal Mid-Atlantic Bight. *Journal of Geophysical Research: Oceans*, *127*, e2022JC018833. https://doi.org/10.1029/2022JC018833

Received 7 MAY 2022
Accepted 21 OCT 2022

Quantification of the Dominant Drivers of Acidification in the Coastal Mid-Atlantic Bight

E. K. Wright-Fairbanks[1] and G. K. Saba[1]

[1]Center for Ocean Observing Leadership, Department of Marine and Coastal Sciences, School of Environmental and Biological Sciences, Rutgers University, New Brunswick, NJ, USA

Abstract In shallow coastal shelves like the Mid-Atlantic Bight (MAB), ocean acidification due to increased atmospheric carbon dioxide (CO_2) is compounded by highly variable coastal processes including riverine freshwater inputs, nutrient loading, biogeochemical influence, coastal currents and water mass mixing, and seasonal transitions in physical parameters. Past deconstructions of carbonate system drivers in the MAB have focused on nearshore zones or single season data, and thus lack the spatial and temporal resolution required to assess impacts to important species occupying the shelf. Deconstructing highly resolved data collected during four seasonal Slocum glider deployments in the MAB, this study uses a Taylor Series decomposition to quantify the influence of temperature, salinity, biogeochemical activity, and water mass mixing on pH and aragonite saturation state from sea surface to bottom. Results show that water mass mixing and biogeochemical activity were the most significant drivers of the carbonate system in the MAB. Nearshore water was more acidic year-round due to riverine freshwater input, but photosynthesis reduced acidity at certain depths and times. Water mass mixing increased acidity in bottom water on the shelf, particularly in summer. Gulf Stream intrusions at the shelf break during fall acted to mitigate acidification on the shelf in habitats occupied by carbonate-bearing organisms. The relationships quantified here can be used to improve biogeochemical forecast models and determine habitat suitability for commercially important fin and shellfish species residing in the MAB.

Plain Language Summary The coastal ocean is experiencing changes in chemistry due to human activities, including carbon dioxide emissions, nutrient runoff, and seasonal changes in temperature, salinity, and coastal currents. These drivers have been studied close to shore and/or only during single seasons, leaving a gap in our understanding of seasonal changes across the entire economically important shelf region. Here, we use high-resolution data collected by a deep-sea robot that measures chemistry from ocean surface to the sea floor. We determined the importance of four key influences (temperature, salinity, water mass mixing, and biological activity) on changes in coastal chemistry over the course of a year. We found that the most important driver of shelf chemistry was mixing of freshwater at the coast and warm, salty water at the edge of the shelf. Biological activity was a secondary influence, which caused smaller scale changes in chemistry. These results can help to predict how coastal chemistry might change in the future, so that we can prepare for the effects on economically important animals and industries.

1. Introduction

Ocean acidification, caused by increasing levels of anthropogenic CO_2 in the atmosphere, is a complex chemical issue that alters the marine carbonate system (Doney et al., 2009; Orr et al., 2005) and threatens calcifying and non-calcifying organisms (Doney et al., 2009, 2020; Kroeker et al., 2013; Saba, Goldsmith, et al., 2019). Ocean acidification has caused measured declines in global ocean pH and the saturation state of aragonite, Ω_{arag}, the soluble form of calcium carbonate used by many marine calcifying organisms. Global open ocean surface pH has decreased by 0.05–0.08 over the last 3 decades (Gledhill et al., 2015; IPCC, 2019) and is projected to continue declining by up to 0.29 pH units over the course of the 21st century (IPCC, 2019; RCP8.5). Global open ocean Ω_{arag} is decreasing at unprecedented rates, and variability in Ω_{arag} is outside the bounds of natural variability, indicating that anthropogenic activity is driving this change (Sutton et al., 2016).

The focus area in this study is the Mid-Atlantic Bight (MAB), which is located within the U.S. Northeast Shelf Large Marine Ecosystem. The MAB has been identified as a net CO_2 sink, meaning it absorbs CO_2 on an annual basis and is therefore subject to acidification patterns observed globally (DeGrandpre et al., 2002). In coastal

shelves like the MAB, ocean acidification is influenced by coastal processes such as riverine freshwater input, biological growth and decay, upwelling, changes in temperature and water column structure, and interactions between coastal currents (Cai et al., 2020; Gledhill et al., 2015; Saba, Goldsmith, et al., 2019; Siedlecki, Pilcher, et al., 2021; Siedlecki, Salisbury, et al., 2021; Wootton et al., 2008). These processes affect acidification on timescales from minutes to years (Runcie et al., 2018; Xu et al., 2017, 2020).

Riverine and estuarine waters feeding into the MAB shelf are lower in salinity and total alkalinity (TA) than seawater, and therefore are more acidic (Kwiatkowski & Orr, 2018). Consequently, surface water where rivers meet the ocean have lower pH and Ω_{arag} than surface seawater further offshore (Cai et al., 2020; Saba, Wright-Fairbanks, et al., 2019; Wright-Fairbanks et al., 2020). Rivers also deliver nutrients to the coastal zone, supporting phytoplankton blooms that lead to the uptake of CO_2 and increased pH in the surface ocean, followed by the release of CO_2 and decreased pH in bottom waters when biological material sinks and is respired (Cai et al., 2011; Wright-Fairbanks et al., 2020). Seasonal stratification in the MAB is significant and traps a subsurface water mass (the Cold Pool) on the shelf in the spring and summer (Houghton et al., 1982; Saba, Wright-Fairbanks, et al., 2019; Wright-Fairbanks et al., 2020; Z. Chen et al., 2018). Lack of ventilation between the Cold Pool and atmosphere during seasonal stratification likely traps respired CO_2 in this subsurface water, contributing to a decline in pH and Ω_{arag} from spring through summer. Wright-Fairbanks et al. (2020) reported seasonal changes in the MAB carbonate system, suggesting potential links to seasonal stratification in the spring and summer, thermodynamic equilibrium, and air-sea gas exchange in near-surface waters, seasonal subsurface phytoplankton blooms, freshwater riverine inputs and precipitation in the nearshore, and the mixing of Gulf-Stream influenced slope water with Labrador-current influenced shelf water at the shelf break. However, these relationships were not quantitatively evaluated.

Drivers of the carbonate system have been investigated at various resolutions in the MAB and nearby Gulf of Maine, but due to a lack of sufficient data, none have quantified drivers over highly resolved space on a seasonal scale. On a decadal scale, interactions between the northward-flowing Gulf Stream and southward-flowing Labrador Current have been shown to influence MAB shelf water properties, including the carbonate system, as they intersect offshore (Grodsky et al., 2017; Saba et al., 2016; Salisbury & Jonsson, 2018; Wanninkhof et al., 2015). The Gulf Stream is warm, salty, and characterized by high pH and Ω_{arag}, while the Labrador Current is cold, fresher, and has lower pH and Ω_{arag} (Grodsky et al., 2017; Saba et al., 2016; Salisbury & Jonsson, 2018; Wanninkhof et al., 2015). Additionally, seasonal temperature and salinity cycles in the MAB can influence regional pH and Ω_{arag} (Cai et al., 2020; Richaud et al., 2016). Monthly sampling programs along shelf and embayment transects have provided physical, biological, and chemical data in surface, bottom, and mid-depth water (10–50 m resolution) (Boehme et al., 1998; Rheuban et al., 2019; Z. Wang et al., 2016). These sampling programs have high temporal resolution, capturing all seasons over multiple years, but lack spatial resolution across the shelf. Conversely, multiple major cruise campaigns (GOMECC-1, 2, ECOA-1, 2,) have conducted carbonate chemistry sampling on cross-shelf transects in the MAB from sea surface to the bottom (10–100 m resolution) (Cai et al., 2020; Xu et al., 2017, 2020), but occur every few years and only in the summer, therefore lacking critical seasonal resolution.

In this study, we quantified the drivers of pH and Ω_{arag} from sea surface to bottom using data from four seasonal deployments of a Teledyne-Webb Slocum G2 glider. The glider is an autonomous underwater vehicle, equipped with a recently developed ISFET-based pH sensor. Along with pH, the glider collects high-resolution measurements of salinity, temperature, depth, dissolved oxygen, and optical properties (e.g., chlorophyll *a* and backscatter), allowing the quantification of carbonate system drivers as they vary seasonally and over space and depth. It is imperative to understand the interactions between drivers of the coastal marine carbonate system to accurately predict and mitigate the effects of acidification on coastal ecosystems. High-resolution data are necessary to detect fine-scale changes in the carbonate system that occur due to biogeochemical and physical influence, especially in the highly dynamic coastal shelf.

2. Materials and Methods

2.1. Data Set Description

Data were obtained from four seasonal glider missions throughout the New Jersey coastal shelf over the course of 2 years (spring 2018, summer 2019, fall 2019, and winter 2019; Figure 1; data available at: http://slocum-data.marine.

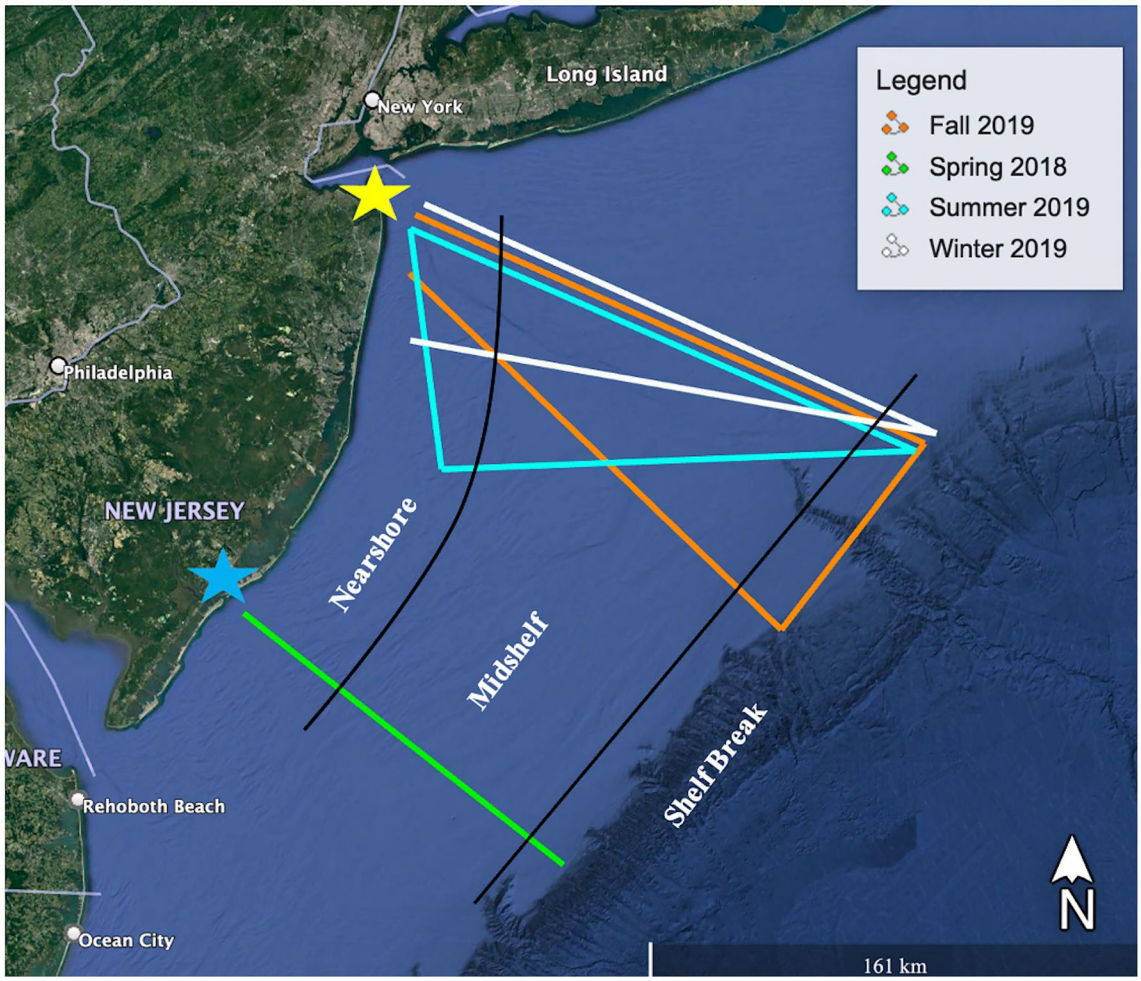

Figure 1. Map of pH glider deployment tracks in the Mid-Atlantic Bight, 2018–2019. A yellow star marks the winter, summer, and fall shore point (Sandy Hook, NJ), and a blue star marks the spring shore point (Atlantic City, New Jersey). Black lines indicate the boundaries between the nearshore, midshelf, and shelf break regions. Produced using Google Earth, with data from SIO, NOAA, U.S. Navy, NGA, and GEBCO, and imaging from Landsat/Copernicus.

rutgers.edu/erddap/search/index.html?page=1%26itemsPerPage=1000%26searchFor=ru30). During each deployment, the glider was equipped with a deep ISFET-based pH sensor integrated into a pumped CTD port located in the glider's science bay (Saba, Wright-Fairbanks, et al., 2019). Additional sensors included an Aanderaa oxygen optode and a Sea-Bird Scientific BB2FL ECO puck used to measure chlorophyll fluorescence, colored dissolved organic matter, and optical backscatter. Concurrent measurements from the glider sensors provided high temporal (0.5 Hz sampling) and spatial (<1 m depth, ~270 profiles over 20 km per day) resolution measurements of biological, physical, and chemical ocean properties over four seasons. Efforts taken to ensure glider sensor data quality were described by Wright-Fairbanks et al. (2020). pH sensor accuracy and field uncertainty were better than ±0.05 pH units and ±0.001 pH units, respectively, for these deployments (Wright-Fairbanks et al., 2020).

Glider-measured variables were used to resolve the marine carbonate system. pH on the total scale was calculated using glider-measured pH reference voltage, temperature, salinity, and pressure. TA was calculated from measured salinity based on season-specific linear relationships between TA and salinity in the MAB (Wright-Fairbanks et al., 2020). TA exhibits near-conservative behavior with respect to salinity in the Atlantic along the east coast of the United States (Cai et al., 2010; Z. Wang et al., 2013). Discrete samples used to derive TA-salinity relationships spanned depths from 0 to 200 m along the MAB shelf, which is the space covered by these glider deployments. Seasonal TA-salinity regressions, with TA in μmol/kg, were:

$$\text{Winter: } TA = (50.80 \pm 0.47) \times \text{Salinity} + (539.79 \pm 15.93) \quad (1)$$

Table 1
Regional and Depth Definitions Used in This Analysis

	Winter	Spring	Summer	Fall
Nearshore				
Near-surface	Top 5 m	Above 13 m	Above 11 m	Above 42 m
Subsurface	Bottom 5 m	Below 13 m	11–38 m	Below 42 m
Deep water	N/A	N/A	Below 39 m	N/A
Midshelf				
Near-surface	Top 5 m	Above 13 m	Above 11 m	Above 42 m
Subsurface	Bottom 5 m	13–45 m	11–45 m	Below 42 m
Deep water	N/A	Below 56 m	Below 45 m	N/A
Shelf break				
Near-surface	Top 5 m	Above 13 m	Above 11 m	Above 42 m
Subsurface	Bottom 5 m	13–120 m	11–100 m	42–80 m
Deep water	N/A	Below 120 m	Below 100 m	Below 88 m

$$\text{Spring: TA} = (49.94 \pm 0.45) \times \text{Salinity} + (572.57 \pm 15.16) \quad (2)$$

$$\text{Summer: TA} = (53.01 \pm 0.63) \times \text{Salinity} + (463.27 \pm 21.19) \quad (3)$$

$$\text{Fall: TA} = (46.17 \pm 0.79) \times \text{Salinity} + (698.00 \pm 26.47) \quad (4)$$

These seasonal TA-salinity regressions are comparable to previously derived regressions. Hunt et al. (2021) derived winter, spring, and summer TA-salinity equations using surface samples from eight cruises in 2017 and 2018 that were equipped with an underway TA analyzer. Their equations had lower slopes (winter, 40.8; spring, 44.1; and summer, 14.5) and higher endmember TA values (winter, 880; spring, 763; and summer, 1726) than those used here. Cai et al. (2010) derived a MAB TA-salinity relationship using full water column samples from GOMECC and OMP cruise campaigns, which resulted in a slope of 46.6 and endmember TA of 767.6 (spring/summer). Brodeur et al. (2019) utilized a TA-salinity relationship from ECOA-1 data, similar to the equations derived here, with a slope of 47.69 and endmember TA value of 640.77 (summer). Cai et al. (2010) identified a weighted average TA endmember for three Mid-Atlantic Rivers (Susquehanna, Connecticut, and Hudson) of 697 µmol/kg during spring/summer. Endmember TA values used in this study are slightly lower than previous studies, likely reflecting samples taken near the Raritan and Delaware River outflows, which are an important component of the study area, and potentially highlighting seasonal differences in endmember chemistry.

pH and TA were used as inputs into CO2SYS for MATLAB (v3.0; Lewis & Wallace, 1998; Orr et al., 2018; van Heuven et al., 2011), along with glider temperature, salinity, and pressure, K1 and K2 constants (Mehrbach et al., 1973) with refits (Dickson & Millero, 1987), KSO_4 constant (Dickson, 1990), KHF dissociation constant (Perez & Fraga, 1987), and borate-to-salinity ratio (Uppstrom, 1974). Variables derived from the CO2SYS program and used in this study were Ω_{arag}, hydrogen ion concentration ($[H^+]$), and dissolved inorganic carbon (DIC). It is important to note that CO2SYS accounts for alkalinity in the forms of carbonate, bicarbonate, borate, $[OH^-]$, $[H^+]$, P, and Si. Other contributors to alkalinity such as organic species are not accounted for, which may cause overestimation of buffering capacity for CO_2 (Sharp & Byrne, 2020; Song et al., 2020). Further investigation of organic alkalinity contributors in this region would improve estimates of buffering capacity.

2.2. Definition of Spatial and Depth Regions

Each seasonal deployment was divided into three spatial and two or three depth regions. Spatial regions were determined based on the distance of the glider from a shore point near the deployment location. In winter, summer, and fall, the shore point was Sandy Hook, New Jersey and in spring, the shore point was Atlantic City, New Jersey. The nearshore region was defined as 0–40 km from the shore point, midshelf was defined as 40–160 km from shore (40–120 km in spring), and the shelf break was defined as >160 km from shore (>120 km in spring), which is beyond the continental shelf. Depth regions were defined as near-surface, subsurface, and deep. The mixed layer was identified as the depth of maximum Brunt-Vaisala frequency squared (N^2) (Carvalho et al., 2017). Near-surface water was considered to be above the mixed-layer depth, while subsurface water was below the mixed layer. In winter, which exhibited a well-mixed water column, pseudo-surface and -bottom regions were defined as the top 5 and bottom 5 m of the water column. Defining these regions in winter allowed consistent analyses of all seasons.

Deep water was identified based on the relationship between depth and sensitivity of carbonate system parameters to changes in driver variables. In a season, all drivers exhibited a change in this relationship at similar depths, indicating differential driver influence beginning at that depth (Figure S1 in Supporting Information S1). Breaks in the slope of these relationships are indicative of deep water mass influence and occurred most often in the deepest water in the midshelf or shelf break in spring, summer, and fall. Additionally, deep water had distinctively different temperature (colder) and salinity (saltier) than subsurface and near-surface water. Overall, 29 seasonal, spatial, and depth regions were defined (Table 1).

2.3. First-Order Taylor Series Decomposition of Ω_{arag} and pH

The mathematical influence of four driver variables (temperature (T), salinity (S), TA, and DIC) on two output variables (Ω_{arag} and pH) was demonstrated using a first-order Taylor Series Decomposition, which has been used previously for similar data sets (Kwiatkowski & Orr, 2018; Rheuban et al., 2019; Xu et al., 2020; Z. Wang et al., 2016). The Taylor Series method is applicable to ocean water, where metrics like DIC, pCO_2, and carbonate saturation sensitivity are not affected by low salinity extremes (Cai et al., 2021).

Anomalies in output variables Y (ΔY) were calculated for each sample compared to a reference value $Y_\circ$

$$\Delta Y = Y - Y_\circ \tag{5}$$

where

$$Y_\circ = Y\left(\overline{T}, \overline{S}, \overline{TA}, \overline{DIC}\right) \tag{6}$$

and $\overline{X}$ represents the mean value of input variables X in the reference condition (X_{ref}).

Here, two analyses are run with different X_{ref} definitions. Analysis 1 defines $\overline{X}$ in one depth region throughout a deployment's full spatial extent (e.g., mean TA in fall near-surface water). Analysis 2 defines $\overline{X}$ in one depth/spatial region throughout all seasonal deployments (e.g., annual mean TA in nearshore near-surface water). Analysis 1 allows for the quantification of spatial variability in carbonate system drivers in each season, while Analysis 2 quantifies the relative importance of drivers over an annual cycle.

A first-order Taylor Series defines the anomaly of an output variable as the sum of driver variable anomalies multiplied by the sensitivity of the output variable Y to changes in each driver variable X, plus nonlinear error (ϵ).

$$\Delta Y = \Sigma \frac{\partial Y}{\partial X} \Delta X + \epsilon \tag{7}$$

ΔX is computed as $X - X_{ref}$, where X is the sample value and X_{ref} is calculated using Analysis 1 or Analysis 2, as described above. Sensitivities are multiplied by ΔX, then summed (Equations 8 and 9).

$$\Delta pH = \frac{\partial pH}{\partial T}\Delta T + \frac{\partial pH}{\partial S}\Delta S + \frac{\partial pH}{\partial TA}\Delta TA + \frac{\partial pH}{\partial DIC}\Delta DIC + \epsilon \tag{8}$$

$$\Delta\Omega_{arag} = \frac{\partial \Omega_{arag}}{\partial T}\Delta T + \frac{\partial \Omega_{arag}}{\partial S}\Delta S + \frac{\partial \Omega_{arag}}{\partial TA}\Delta TA + \frac{\partial \Omega_{arag}}{\partial DIC}\Delta DIC + \epsilon \tag{9}$$

The sensitivities of Ω_{arag} and H^+ to temperature, salinity, TA, and DIC ($\frac{\partial Y}{\partial T}$, $\frac{\partial Y}{\partial S}$, $\frac{\partial Y}{\partial TA}$, and $\frac{\partial Y}{\partial DIC}$) were derived explicitly using the derivnum.m subroutine of CO2SYS (v.3.0) (Lewis & Wallace, 1998; Orr et al., 2018; Sharp et al., 2020; van Heuven et al., 2011). The derivnum.m subroutine calculates partial derivatives of output carbonate variables to two carbonate inputs (here, TA and DIC), temperature, salinity, nutrients, ammonium, hydrogen sulfide, dissociation constants, and total boron by introducing a small perturbation in one input variable and determining the change in each output variable as calculated using CO2SYS. Error propagation through CO2SYS caused an error in Ω_{arag} of ~0.1 and an error in H^+ of ~0.001. These errors should not affect the relative magnitude of each driver in the sensitivity analysis. H^+ sensitivities were used to calculate pH anomalies according to the established relationship between the two variables (Equation 10).

$$\mathrm{pH} = -\log\left[\mathrm{H}^+\right] \tag{10}$$

Results from this analysis are reported as the numerical influence of each driver variable on each output variable (i.e., the value of $\frac{\partial Y}{\partial X}\Delta X$). For example, the influence of temperature on pH $\left(\frac{\partial pH}{\partial T}\Delta T\right)$ is discussed as ΔpH_T and the influence of salinity on $\Delta\Omega_{arag}$ $\left(\frac{\partial \Omega_{arag}}{\partial S}\Delta S\right)$ is discussed as $\Delta\Omega_S$. These terms allow a comparison of the relative influence of each driver on each output variable. A negative ΔY_X indicates that X acts to decrease Y relative to the mean and a positive ΔY_X indicates that X increases Y.

Marine TA and DIC are altered by biogeochemical processes such as photosynthesis, respiration, $CaCO_3$ dissolution and precipitation, physical mixing of water masses, and air-sea gas exchange (DIC only). The influence of air-sea gas exchange in each season was assessed by simulating changes in mixed layer pCO_2 and DIC assuming air-sea flux was the only driver of change. Gas exchange in each season was calculated using the methods of Wanninkhof (1992), where

$$F = k \times s \times \Delta pCO_2 \tag{11}$$

$$k = 0.31 \times U^2 \times \frac{Sc}{660}^{-0.5} \tag{12}$$

where, s is solubility, U is wind speed, and Sc is the Schmidt number, which takes into account seasonal average sea surface temperature and salinity. ΔpCO_2 between the sea surface and atmosphere was calculated using pCO_2 as estimated in glider deployments and an estimate of atmospheric pCO_2 (403 ppm; based on Mauna Loa annual average ppm). pCO_2 disequilibrium and seasonal average wind speed from the U.S. Wind Climatology (NCEI) were used to quantify the changes in surface layer pCO_2 and DIC caused by gas exchange, and the half-life of equilibration time. The half-life of equilibration time is determined as the time it takes to reach the halfway point between air and sea pCO_2. Full equilibration time, or the time it takes to reach equilibrium between atmospheric and sea surface pCO_2, is represented by an asymptotic function and is therefore difficult to quantify.

In spring and fall, changes in pCO_2 and DIC were small (<3 μatm and <2 μmol/kg), therefore air-sea gas exchange was minor. In winter, pCO_2 and DIC changed significantly but the half-life of equilibration time was 146 days, indicating that gas exchange was minor at a seasonal time scale. Summer showed significant changes in pCO_2 and DIC at a seasonal scale (half-life of equilibration = 46 days, likely due to shallow mixed layer and high wind speeds), indicating significant air-sea exchange. Therefore, gas exchange is considered in the analysis of summer surface water but excluded in the remaining seasons and regions.

The sensitivity of output variables to biogeochemical (BGC), mixing (MIX), and gas exchange influence was calculated based on changes in TA and DIC. Along the western Atlantic coast, TA is dominated by two-endmember horizontal mixing between riverine inputs and coastal seawater (Cai et al., 2010; Jiang et al., 2014). Non-mixing factors that might also influence TA include carbonate dissolution, calcification, and denitrification. There was little evidence of carbonate dissolution or calcification in any season (Figure 2). Denitrification in sediments has been shown to occur in the MAB, altering TA and therefore air-sea gas exchange (Fennel et al., 2008; Seitzinger, 1988; Seitzinger & Giblin, 1996). The seasonal glider data sets do not include nutrient measurements, so it is difficult to identify areas of potential denitrification. However, any changes in TA due to denitrification would disperse throughout the entire water column, dampening their effects. Additionally, conditions in the water column were not optimal for denitrification due to sufficient oxygen levels. Thus, changes in TA (ΔTA) were attributed solely to water mass mixing.

To separate changes in DIC due to biogeochemistry, air-sea gas exchange, and water mass mixing, DIC was normalized following the method of Friis et al. (2003),

$$n\text{DIC} = \frac{\text{DIC}_{\text{spl}} - \text{DIC}_{\text{Sal=0}}}{\text{Sal}_{\text{spl}}} \times \text{Sal}_{\text{ref}} + \text{DIC}_{\text{Sal=0}} \tag{13}$$

where Sal_{spl} is the sample salinity, Sal_{ref} is the reference salinity as used in Equation 6, and $\text{DIC}_{\text{Sal=0}}$ is DIC in the freshwater endmember. The value of DIC at the freshwater endmember was the y-intercept of the TA-salinity equation derived for each season, under the assumption that TA ≈ DIC at zero salinity (Zeebe & Wolf-Gladrow, 2001). While a DIC-salinity regression was derived, the endmember values for each season had a greater error than those of the TA-salinity regression. Normalizing DIC using the TA endmember changed nDIC by a maximum of 0.4% compared to nDIC calculated using the DIC endmember. TA-salinity equations incorporated data from 0 to 200 m, so they were used to calculate nDIC for surface, bottom, and deep water.

Normalization to a reference salinity removes the effect of conservative mixing from DIC, meaning ΔnDIC (nDIC – DIC_ref) represents the change in DIC due to biogeochemical factors. The BGC term also includes the effects of air-sea gas exchange in summer surface water, but it is referred to as BGC for continuity. The sensitivity of output variables to BGC was determined explicitly as $\frac{\partial Y}{\partial n\text{DIC}}$ using the derivnum.m subroutine of CO2SYS.

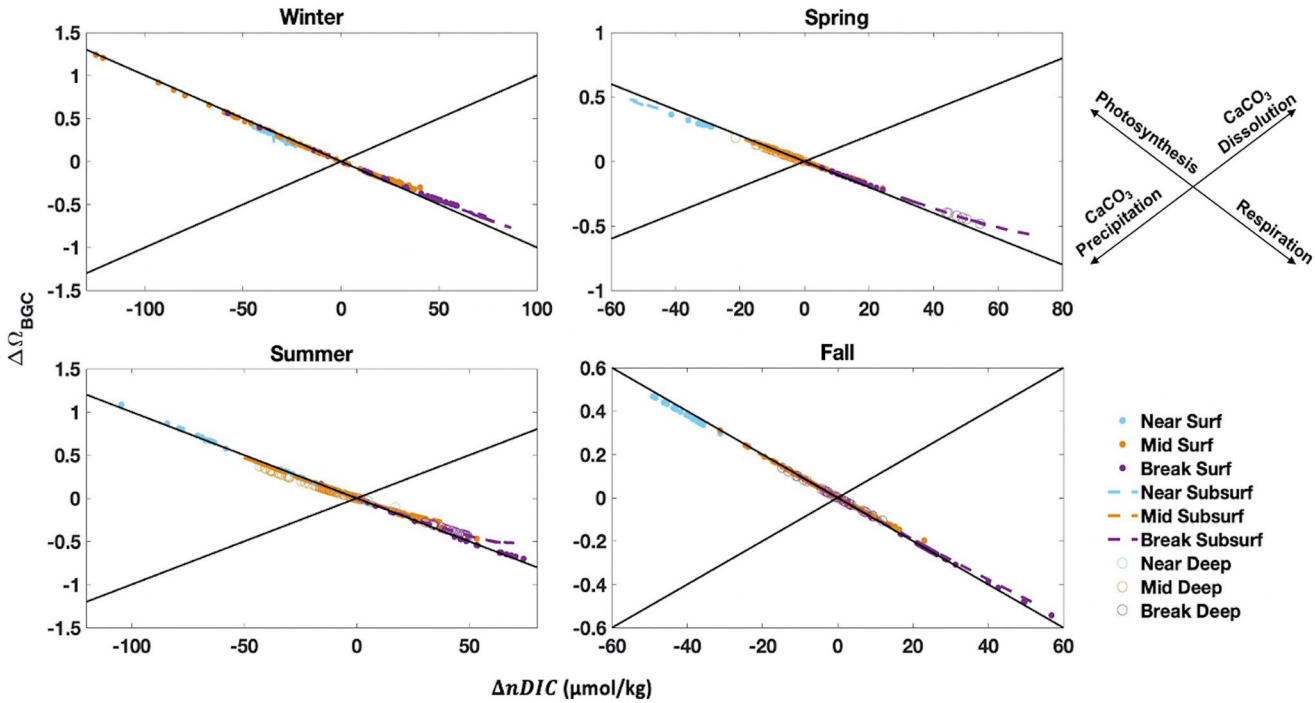

Figure 2. $\Delta nDIC$ versus $\Delta\Omega_{BGC}$ in all four seasons. Black lines represent the theoretical relationship between $\Delta nDIC$ and $\Delta\Omega_{BGC}$ if only photosynthesis/respiration and/or $CaCO_3$ dissolution/precipitation occur. Deviations from the photosynthesis-respiration line are minor in shelf break subsurface water (all seasons) and nearshore surface water (spring).

$$\Delta Y_{\mathrm{BGC}} = \frac{\partial Y}{\partial n\mathrm{DIC}} \Delta n\mathrm{DIC} \tag{14}$$

$$\text{Summer}: \Delta Y_{\mathrm{BGC+air-sea}} = \frac{\partial Y}{\partial n\mathrm{DIC}} \Delta n\mathrm{DIC} \tag{15}$$

The change in output variables due to water mass mixing altering DIC was then calculated as follows:

$$\Delta Y_{\mathrm{DIC_{MIX}}} + \varepsilon = \Delta Y - \Delta Y_T - \Delta Y_S - \Delta Y_{\mathrm{BGC}} - \Delta Y_{\mathrm{TA}} \tag{16}$$

and $\Delta Y_{\mathrm{DIC_{MIX}}} + \varepsilon$ were added to ΔY_{TA} determine the overall change in output variables caused by water mass mixing.

$$\Delta Y_{\mathrm{MIX}} = \Delta Y_{\mathrm{TA}} + \Delta Y_{\mathrm{DIC_{MIX}}} + \varepsilon \tag{17}$$

In this deconvolution, ε accounts for nonlinear effects on the carbonate system and other unidentified processes. The cumulative error of nonlinear effects by allowing only one input to vary at a time was less than 0.005 in Ω_{arag} and less than 0.01 in pH in each season, meaning ε is likely inconsequential.

Final algorithms to calculate output variable anomalies were as follows:

$$\Delta pH_{\mathrm{tot}} = \Delta pH_T + \Delta pH_S + \Delta pH_{\mathrm{BGC}} + \Delta pH_{\mathrm{MIX}} + \epsilon \tag{18}$$

$$\Delta\Omega_{\mathrm{tot}} = \Delta\Omega_T + \Delta\Omega_S + \Delta\Omega_{\mathrm{BGC}} + \Delta\Omega_{\mathrm{MIX}} + \varepsilon \tag{19}$$

To assess the significance of drivers, we discuss the driver influence using three definitions: minor influence ($|\Delta\Omega_X| \leq 0.05$ and $|\Delta\mathrm{pH}_X| \leq 0.03$), moderate influence ($|\Delta\Omega_X| = 0.05 - 0.50$ and $|\Delta\mathrm{pH}_X| = 0.03 - 0.15$), and major influence ($|\Delta\Omega_X| > 0.50$ and $|\Delta\mathrm{pH}_X| > 0.15$). Driver values were non-normally distributed (Shapiro-Wilks test; visual examination of quantile-quantile plot). Therefore, these bounds were set using percentiles, where minor influence was below the 50th percentile, moderate influence was between the 50th and 90th percentile, and major influence was 90th percentile or above.

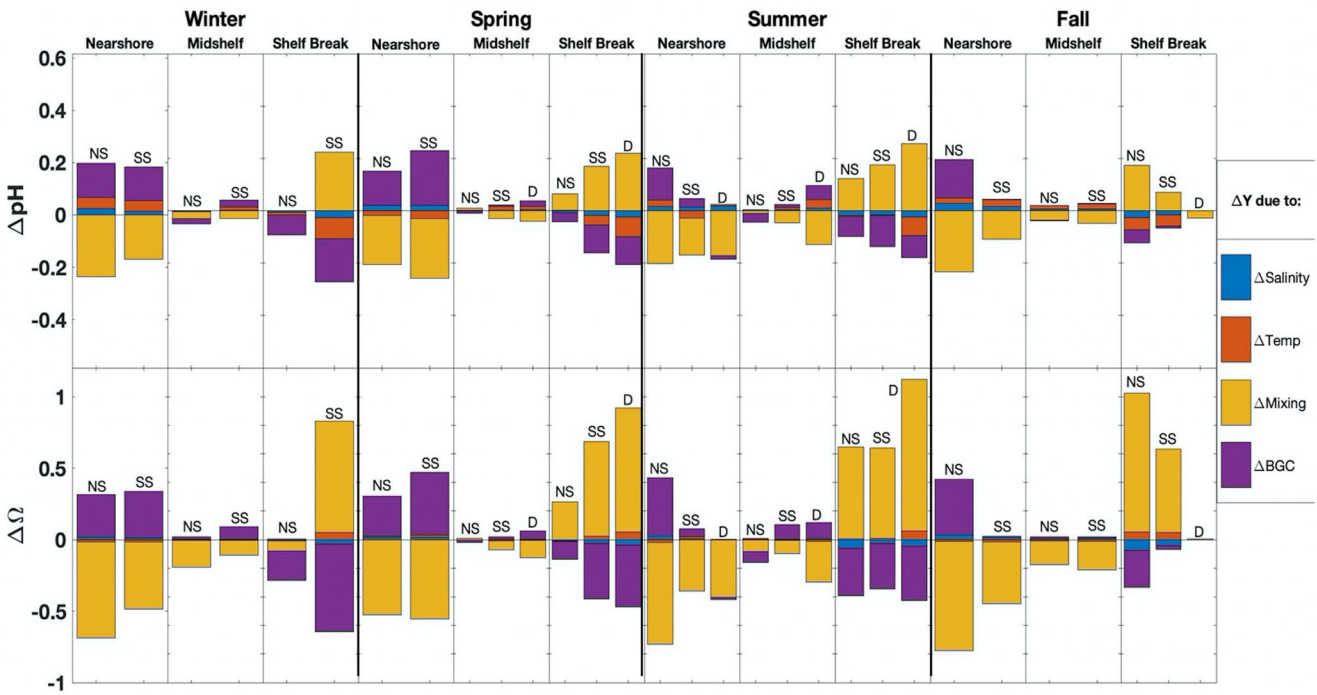

Figure 3. Stacked bar graphs indicating the influence of each driver (temperature, salinity, mixing, and biogeochemistry) on changes in pH and Ω_{arag} compared to a seasonal mean (Analysis 1). Data are shown separated by distance from shore (nearshore, midshelf, and shelf break) and individual bars are labeled with depth (NS: near surface, SS: subsurface, and D: deep).

3. Results

Glider data exhibited seasonal, spatial, and depth variability in biological, physical, and chemical ocean properties. Likewise, physical and biological drivers of the carbonate system varied spatially and seasonally. Sensitivities of each response variable to the various drivers and property anomalies from seasonal and annual means are reported (Tables S1–S3 in Supporting Information S1).

3.1. Analysis 1: Season-Specific Spatial Variability in Drivers

Carbonate system drivers varied in influence between the nearshore, midshelf, and shelf break in each depth region and season (Figure 3; Table S2 in Supporting Information S1). We describe results from Analysis 1 below.

Winter near-surface water displayed little variation in Ω_{arag} or pH over the spatial extent of deployment. The influences of water mass mixing and biogeochemistry on Ω_{arag} and pH were moderate to major but opposite in sign, canceling each other out. Temperature and salinity had minor influence on surface Ω_{arag} (-0.02 to 0.02 in all regions), and minor to moderate (-0.01 to 0.04 in all regions) influence on pH (Figure 3).

Winter subsurface Ω_{arag} and pH varied spatially, with shelf break Ω_{arag} more positive and pH more negative than the shelf regions. Positive subsurface $\Delta\Omega_{tot}$ at the shelf break was driven by major positive mixing influence (0.78 ± 0.03, $n = 34$). Negative ΔpH_{tot} at the shelf break was driven by major negative biogeochemical (-0.17 ± 0.03, $n = 34$), moderate negative temperature (-0.08 ± 0.02, $n = 34$), and minor negative salinity influences (-0.03 ± 0.01, $n = 34$), which offset major positive ΔpH_{MIX} (0.22 ± 0.01, $n = 34$) (Figure 3).

Spring, summer, and fall near-surface and sub-surface $\Delta\Omega_{tot}$ were negative in the nearshore and positive at the shelf break, and the midshelf often acted as a transition zone between the two. This pattern followed the sign of $\Delta\Omega_{MIX}$, indicating that water mass mixing was the most important driver of Ω_{arag} spatial variability (Figure 3). As such, spring, summer, and fall were influenced by mixing of a low-Ω_{arag} water mass in the nearshore and high-Ω_{arag} mixing at the shelf break. Finer-scale variability in $\Delta\Omega_{tot}$ corresponded to changes in biogeochemistry

or gas exchange (summer only). For instance, a positive BGC/gas exchange influence from 100 to 160 km offshore in summer caused positive $\Delta\Omega_{tot}$, deviating from water mass mixing influence.

Spring and fall near-surface and sub-surface pH experienced little spatial variability (Figure 3). In all regions, water mass mixing was balanced by a combination of opposite biogeochemical, temperature, and/or salinity influence. Summer surface pH anomalies were also minor or moderate (−0.04 to 0.01), driven by the balance between biogeochemistry/air-sea gas exchange and water mass mixing (Figure 3). Summer subsurface pH anomaly was moderately negative from shore to 100 km offshore, driven by water mass mixing and biogeochemistry. Further than 100 km from shore, summer ΔpH_{tot} was positive, driven by biogeochemistry in the midshelf and mixing at the shelf break.

A deep-water mass was identified in spring (midshelf and shelf break), summer (nearshore, midshelf, and shelf break), and fall (shelf break). In spring and summer, shelf break deep water exhibited a positive Ω_{arag} anomaly compared to other spatial regions due to major positive $\Delta\Omega_{MIX}$ (spring: 0.73 ± 0.01, $n = 18$; summer: 1.06 ± 0.01, $n = 18$; Figure 3). Both seasons exhibited negative $\Delta\Omega_{BGC}$ in shelf break deep water and positive $\Delta\Omega_{BGC}$ in the midshelf. Spring and summer deep water showed little evidence of carbonate dissolution or precipitation, meaning biogeochemical influence can be attributed to photosynthesis and respiration (Figure 2). Positive $\Delta\Omega_{BGC}$ in the midshelf indicated the relative importance of deep water photosynthesis and negative $\Delta\Omega_{BGC}$ at the shelf break indicated deep water respiration. Spring and summer deep water pH also experienced major positive influence of water mass mixing at the shelf break (spring: 0.17 ± 0.00, $n = 82$; summer: 0.26 ± 0.00, $n = 39$).

The deep-water mass identified at the shelf break in fall exhibited a minor negative ΔpH_{tot} (-0.03 ± 0.01, $n = 39$). Though fall deep water only occurred in one spatial region, a pH anomaly can appear because anomalies were calculated using reference values (Equation 6) instead of mean pH values, reflecting the nonlinear nature of thermodynamic equations (Rheuban et al., 2019).

3.2. Analysis 2: Seasonal Variability in Drivers

Analysis 2 revealed that carbonate system drivers varied between seasons in the MAB (Table S3 in Supporting Information S1). Complete results showing the balance of drivers in each spatial and depth region are found in Figure 4. Here, we highlight seasonal changes in water column features that influence the carbonate system.

Analysis 1 revealed that nearshore near-surface water in every season had negative Ω_{arag} and pH anomalies driven mainly by low-salinity water mass mixing. Analysis 2 showed that of all seasons, summer nearshore near-surface water was most influenced by mixing, as it exhibited the most negative $\Delta\Omega_{MIX}$ (-0.83 ± 0.26, $n = 28$; Table S3 in Supporting Information S1; Figure 5) and ΔpH_{MIX} (-0.32 ± 0.11, $n = 28$; Table S3 in Supporting Information S1; Figure 5). Conversely, fall nearshore near-surface water had the most positive $\Delta\Omega_{MIX}$ (0.61 ± 0.02, $n = 21$; Table S3 in Supporting Information S1; Figure 5) and ΔpH_{MIX} (0.16 ± 0.01, $n = 21$; Table S3 in Supporting Information S1; Figure 5).

Negative $\Delta\Omega_{tot}$ compared to an annual mean is characteristic of the Cold Pool and was evident in the midshelf region in spring and summer (subsurface and deep). Spring (deep) and summer (subsurface and deep) also exhibited a negative pH anomaly in the midshelf (spring deep: -0.02 ± 0.00, $n = 80$; summer subsurface: -0.09 ± 0.06, $n = 120$; summer deep: -0.11 ± 0.03, $n = 120$). In summer, these anomalies were driven by negative $\Delta\Omega_{MIX}$ (-0.97 to -0.40) and ΔpH_{MIX} (-0.14 to -0.12) while biogeochemical influence caused deviations of ΔY_{tot} from ΔY_{MIX} (Figure 6). In spring, the negative Ω_{arag} anomalies were driven by additive negative mixing and biogeochemistry (Figure 6).

Positive surface ΔpH_{tot} was evident when averaged across all regions in winter (0.07 ± 0.04, $n = 187$) and negative surface ΔpH_{tot} was evident across all regions in summer (-0.05 ± 0.02, $n = 188$) when compared to an annual mean (Figure 7). On the other hand, surface $\Delta\Omega_{tot}$ was negative in winter (-0.28 ± 0.24, $n = 187$) and positive in summer (0.26 ± 0.19, $n = 188$). Drivers influencing these differential patterns are shown in Figure 7. Summer $\Delta\Omega_{tot}$ was driven by the balance between major biogeochemical/air-sea gas exchange and mixing influences. In winter, the negative or near-zero Ω_{arag} anomaly was also driven by BGC and mixing. Positive ΔpH_{tot} in winter was driven by moderate to major temperature influence, while negative ΔpH_{tot} in summer was driven by mixing and counteracted by BGC/air-sea gas exchange.

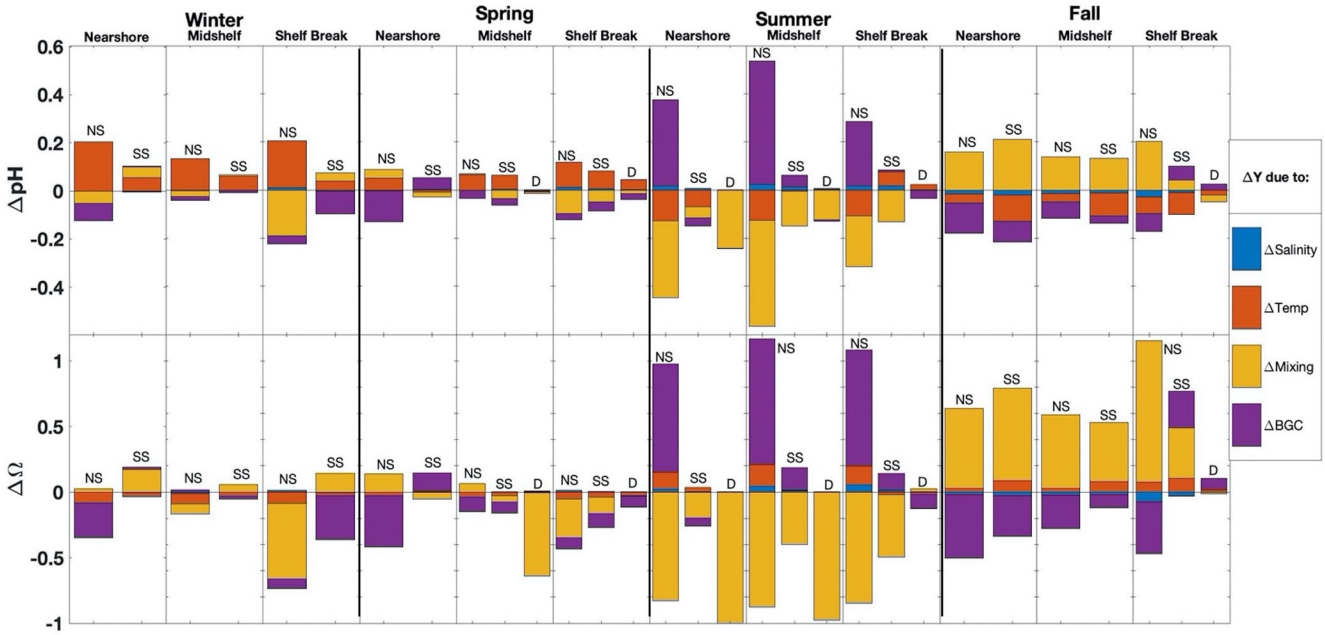

Figure 4. Stacked bar graphs indicating the influence of each driver (temperature, salinity, mixing, and biogeochemistry) on changes in pH and Ω_{arag} compared to an annual mean (Analysis 2). Data are shown separated by distance from shore (nearshore, midshelf, and shelf break) and individual bars are labeled with depth (NS: near surface, SS: subsurface, and D: deep).

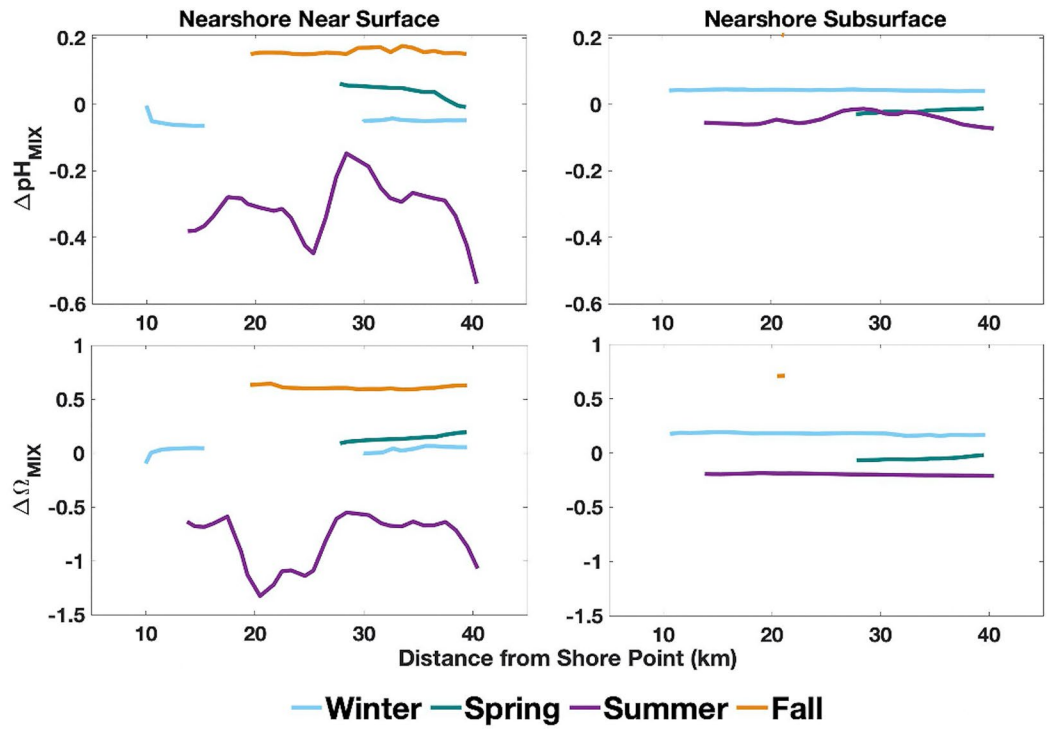

Figure 5. Relative influence of water mass mixing on Ω_{arag} and pH in the nearshore region in four seasons. ΔY_{MIX} was calculated as the difference from an annual mean value in the nearshore surface and/or bottom water (Analysis 2). A robust loess smoothing filter, spanning 10% of the data points, was applied for visualization purposes.

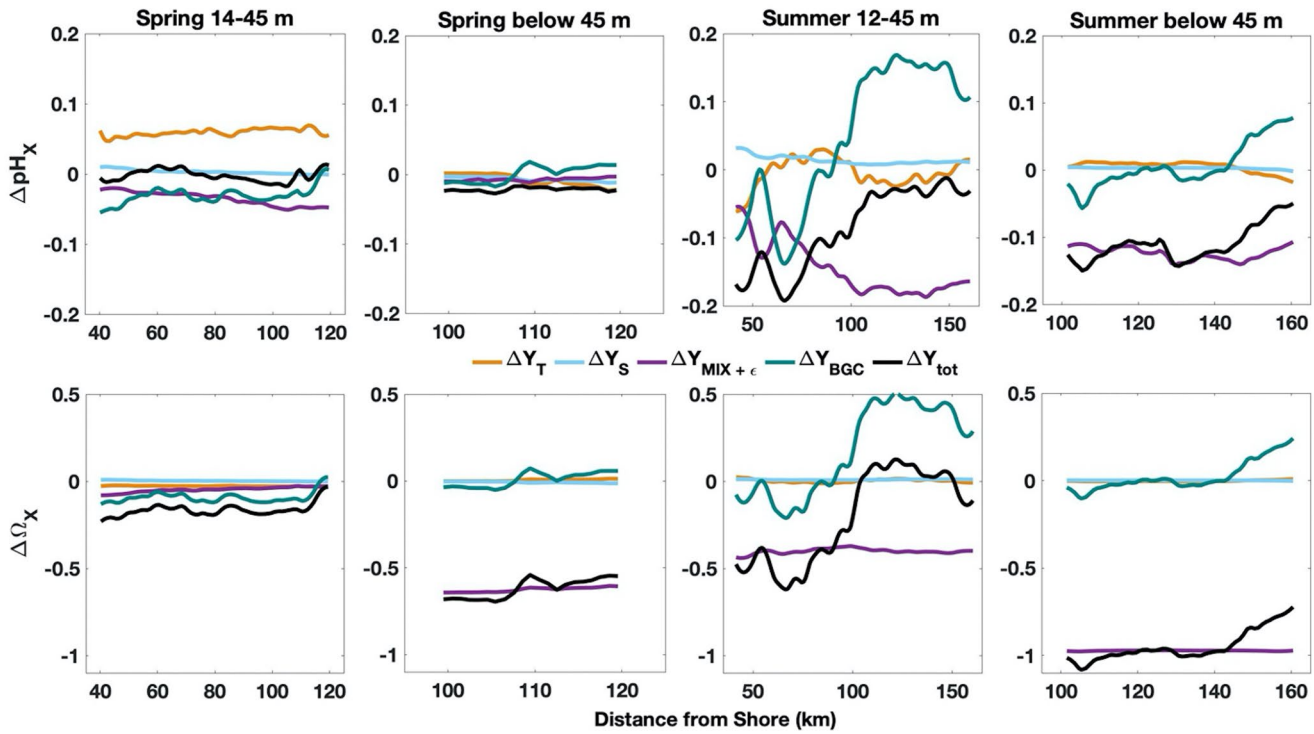

Figure 6. Drivers of change in Ω_{arag} and pH in Cold Pool-area water. ΔY_X is reported relative to the annual mean (Analysis 2). ΔY_{tot} is the resulting sum of all driver influences. Negative $\Delta\Omega_{tot}$ and ΔpH_{tot} are characteristic of Cold Pool carbonate chemistry patterns. A robust loess smoothing filter, spanning 10% of the data points, was applied for visualization purposes.

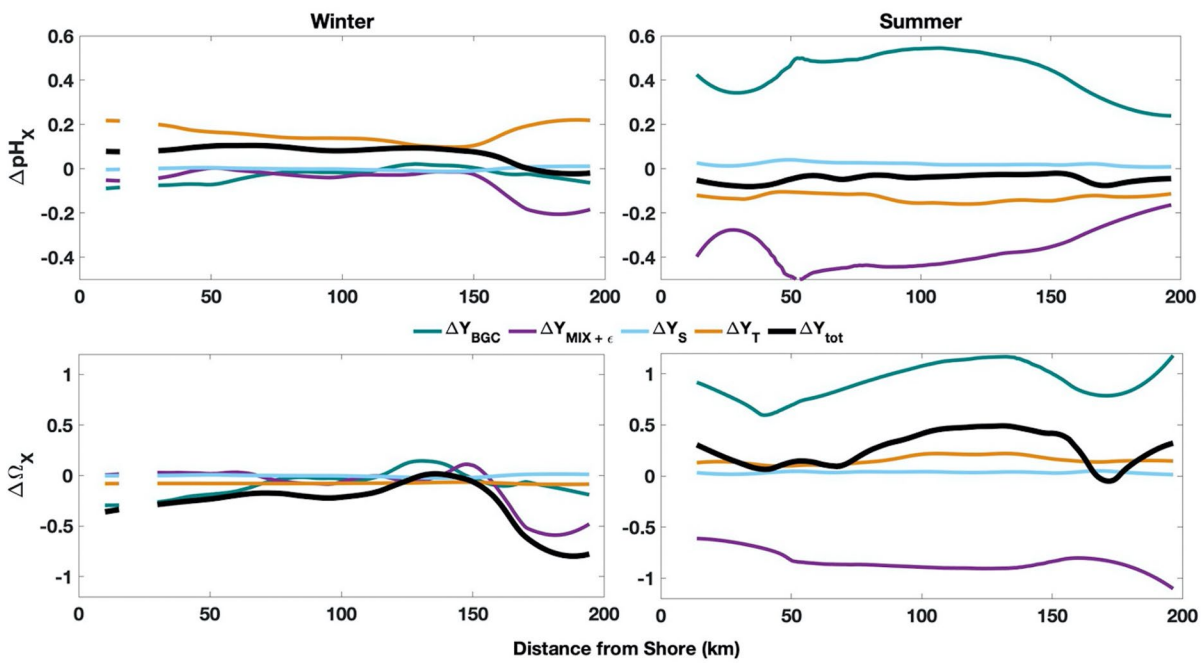

Figure 7. Drivers of change in Ω_{arag} and pH in shelf surface water in winter and summer 2019, compared to an annual average (Analysis 2). ΔY_{tot} is the resulting sum of all driver influences. A robust loess smoothing filter, spanning 10% of the data points, was applied for visualization purposes.

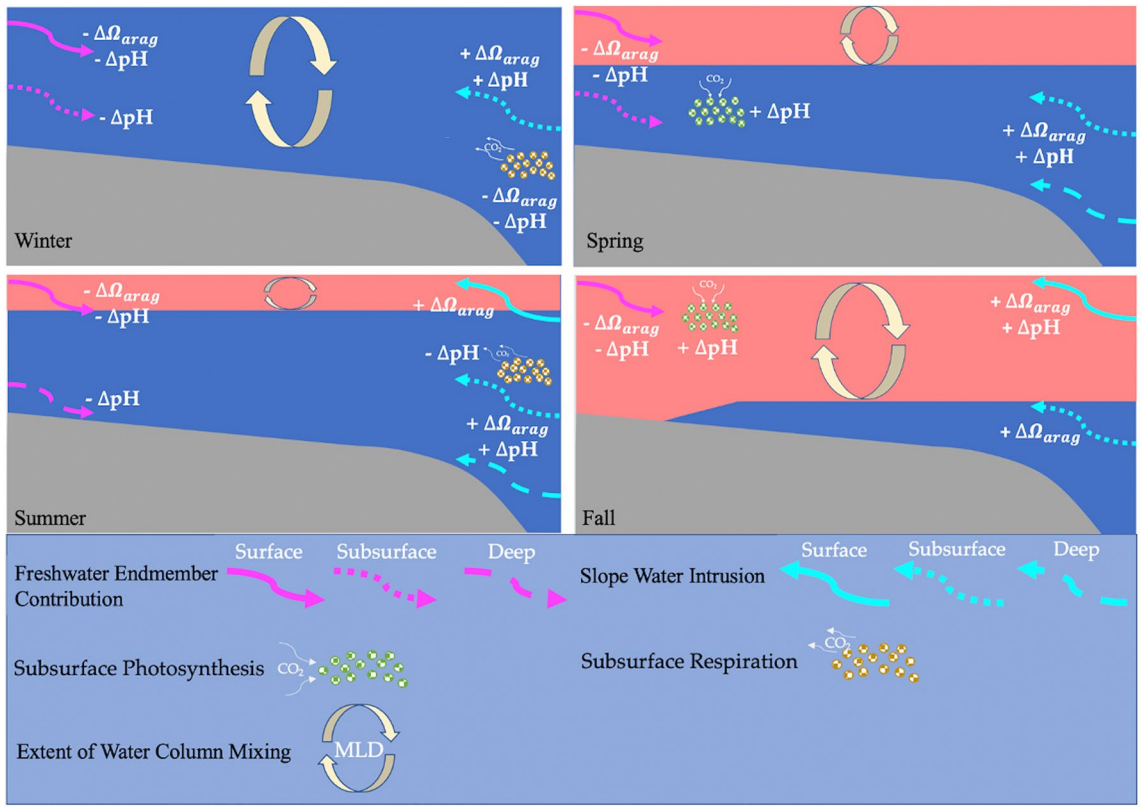

Figure 8. Schematic depiction of the major drivers of Ω_{arag} and pH in each season. Major drivers were identified as those which changed $\Delta\Omega_{arag}$ >0.50 and pH >0.15 (90th percentile; see Section 4.3.3). Red indicates the approximate surface mixed-layer depth in each season.

4. Discussion

The decomposition of carbonate system drivers identified distinct oceanographic features influencing seasonal and spatial dynamics of acidification in the MAB (Figure 8). In looking at the two analyses, we are able to track differences in drivers along a spatial gradient but also cross-reference each spatial zone (cross-shelf and depth) to its reference condition over the course of a year. Water mass mixing was the primary driver of variability in Ω_{arag} and pH, while biogeochemical activity often had a lesser influence on the response variables. Temperature and thermodynamic salinity influence were, more often than not, small in magnitude and equal-but-opposite, meaning the effect of one canceled out the effect of the other. Though changes in salinity indicate water mass mixing, thermodynamic salinity changes were less impactful than mixing due to the smaller range of salinity values compared to TA values. Changes in salinity versus changes in pH and Ω_{arag} are presented in Figure S2 in Supporting Information S1. Quantitative deductions of spatial and seasonal variability in complex carbonate system drivers allow the identification of important ocean properties, processes, and source waters that influence the location and timing of acidification in this system.

4.1. Water Mass Mixing

Multiple modes of water mass mixing likely played a role in seasonal and spatial variability in the carbonate system. The nearshore MAB experiences upwelling, downwelling, and cross-shelf flow regimes due to sustained along-shore southwest winds in the summer, northwest winds in the winter, and southwest, northwest, and northeast winds in both spring and fall (Gong et al., 2010). The region as a whole experiences alongshore flow from north to south via the Labrador Coastal Current (Z. Wang et al., 2013). Local mixing between the Labrador Current and other water masses, like the Gulf Stream, can influence physical and chemical coastal properties. In the nearshore, tidal action and river runoff have a potential mixing influence year-round. At the shelf break, water mass mixing may be driven by eddy interactions with the shelf break jet or internal wave action. Submarine canyons in the MAB experience upwelling of slope water due to wind stress and eddy action, which can lead to the

formation of dense slope water plumes along the shelf (H. Wang, 2021). Lastly, storms influence water column mixing seasonally with tropical storms affecting the MAB in summer and extra-tropical cyclones (nor'easters) more prominent in fall, winter, and early spring. Taken together, these modes of mixing can greatly influence MAB chemistry. The major water mass interactions observed during this study (freshwater endmember mixing, slope water mixing, and Cold Pool water mass exchange) are discussed in detail below (Sections 4.1.1–4.1.3).

4.1.1. Freshwater Influence

In the nearshore, all seasons exhibited lower-than-seasonal-average Ω_{arag} driven by water mass mixing, indicating that a low-alkalinity water mass was influencing the system. This water likely originated from riverine inputs to the system. Sandy Hook, New Jersey, the shore point in winter, summer, and fall, is located near the intersection of the Raritan Bay and Lower New York Bay, two major freshwater influences in the coastal MAB (Figure 1). The spring shore point, Atlantic City, New Jersey, is adjacent to Great Bay and Great Egg Harbor and ∼70 km northeast of the Delaware Bay mouth (Figure 1). Due to the southward-flowing coastal current in this region, riverine discharge is transported southward alongshore (Chant et al., 2008). Offshore wind stress can cause river plume bulging and an offshore plume position (Chant & Jurisa, 2013), but in our study, this was all captured in the nearshore region. Proximity to bays and river plume influence allows mixing of low-alkalinity freshwater into nearshore coastal near-surface water, decreasing Ω_{arag} and pH. Freshwater mixing influence was partially counteracted by nearshore photosynthesis in each season which removed CO_2 from the water column, in turn increasing Ω_{arag} and pH. The acidifying effects of freshwater mixing nearshore extended into the subsurface in spring, summer, and fall.

Coastal ocean mixing with freshwater sources in the nearshore was most influential in the summer. Historically, rivers draining into the MAB exhibit peak outflow during spring, and coastal waters have the lowest salinity in summer, when the cumulative influence of seasonal runoff and precipitation are greatest (Manning, 1991; Whitney, 2010). During the summer glider deployment, multiple large precipitation events caused higher than average rainfall while the glider was in the nearshore and midshelf (17–22 July 2019; https://weather.gov/marfc/precipitation_departures/). This increase in rainfall caused salinity to decrease to ∼29 PSU, which is lower than average climatology levels for the 30-m isobath off coastal New Jersey (30–32 PSU; Fleming, 2016). Low salinity was linked to low TA, Ω_{arag}, and pH in surface waters (Wright-Fairbanks et al., 2020). The negative pH and Ω_{arag} anomalies in summer nearshore surface water demonstrate that high-precipitation events in the MAB can directly influence coastal buffering capacity for CO_2. It is important to note that salinity in these deployments was, on average, no less than 29 PSU, meaning carbonate sensitivity to salinity was not as extreme as it would be in an estuarine environment (Cai et al., 2021).

4.1.2. The Shelf Break Front

The Gulf Stream carries warm, high-salinity water from the equatorial region northward along the U.S. East Coast. Though the Gulf Stream does not interact directly with the MAB coastal shelf, it does influence the slope sea via the shelf break front, which acts as a heat source for the shelf via eddy heat flux (K. Chen & He, 2010). The Gulf Stream also periodically delivers heat and salt to the MAB shelf via warm core rings that break off of meanders north and west of the Gulf Stream deflection point near Cape Hatteras, North Carolina (Andres, 2016). When warm core rings hit the MAB shelf, salt and heat are transferred onto the shelf at a magnitude 6–9x larger than long-term average exchange (K. Chen et al., 2014).

The influence of the Gulf Stream was especially important at the shelf-slope boundary in our study, as evidenced by high Ω_{arag} and pH in spring, summer, and fall near-surface and subsurface shelf break zones compared to the rest of the shelf (Analysis 1; Figure S3 in Supporting Information S1). While mixing of shelf water with high-Ω_{arag} slope water influenced the shelf break carbonate system relative to other coastal processes in spring, summer, and fall, that mixing was most impactful in fall (Analysis 2; Figure 9). A Gulf Stream intrusion onto the shelf was visible in satellite sea surface temperature observations when the glider was at the shelf break during this time (Figure 10). This intrusion brought water with salinity >35 PSU to the 60 m isobath on the shelf, exceeding the climatological average of shelf break front intrusion for summer in the MAB (∼75 m; Linder & Gawarkiewicz, 1998). The salinity of this intrusion was higher than average for MAB shelf break waters in summer (33.5 PSU; Fleming, 2016). The identification of this feature provided a direct link between Gulf Stream intrusion and delivery of high Ω_{arag} water to the MAB shelf.

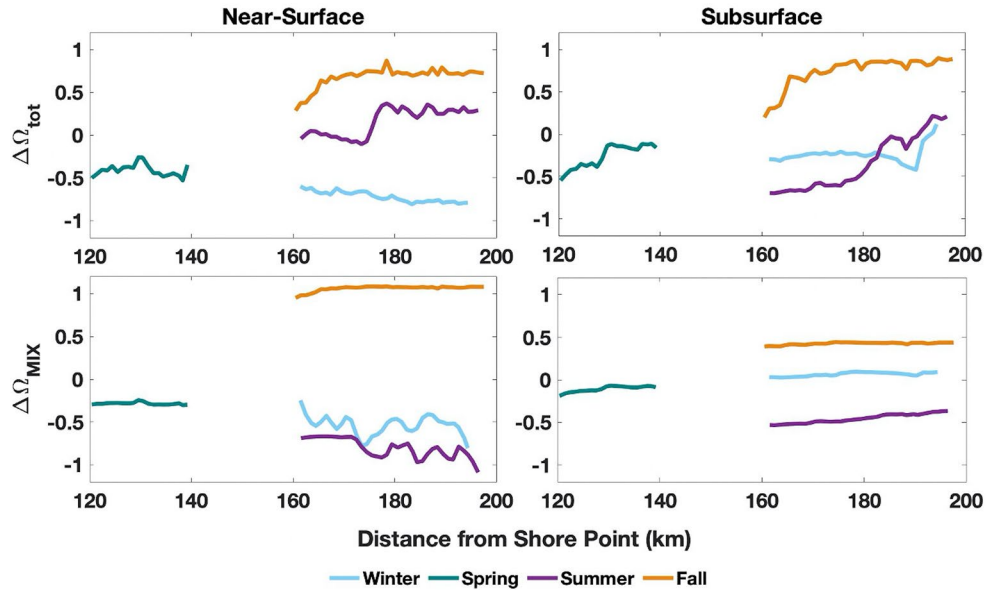

Figure 9. Relative change in Ω_{arag} at the shelf break in each season, compared to an annual mean (Analysis 2). Top panels indicate the total resulting sum of all driver influences and bottom panels show the influence of mixing on Ω_{arag}. Mixing of the high-Ω_{arag} shelf break jet water had the most influence during fall deployment. A robust loess smoothing filter, spanning 10% of the data points, was applied for visualization purposes.

Changes in carbonate chemistry due to Gulf Stream influence in the northeast United States have been recorded previously. From 2005 to 2015, a northward shift in the Gulf Stream related to wind variability and moderately influenced by North Atlantic Oscillation (NAO) caused an increase in sea surface salinity in the Northwest Atlantic (Grodsky et al., 2017). This brought high TA water to the MAB shelf, which counteracted DIC increases and caused a slowdown in the decades-long decline of Ω_{arag} (Xu et al., 2020). Salisbury and Jonsson (2018) recorded an extreme warming (0.2°C increase yr^{-1}) and increased salinity (~0.2 PSU yr^{-1}) event in the Gulf of Maine from 2005 to 2014, which was linked to the weakening of AMOC. During that time period, warming and increasing salinity exhibited a 2.5 times stronger effect on Ω_{arag} than ocean acidification, mitigating the effects of acidification despite a 40+ year trend of decreasing pH and Ω_{arag} due to increased pCO_2 and decreased TA. Based on our sensitivity analysis and links between the Labrador Current, Gulf Stream, and the MAB, a similar event structure could occur in the MAB.

Interestingly, shelf water mixing with slope water did not lead to a major positive pH anomaly in any season because it was counterbalanced by biogeochemical activity and/or temperature. Though mixing of the shelf break jet caused high Ω_{arag} at the edge of the shelf, respiration and temperature had a greater impact on pH compared to the near shore and midshelf regions. Differences in drivers of pH and Ω_{arag} are discussed further in Section 4.2.

At the shelf break, a deep water mass was identified in spring, summer, and fall. This water mass aligns with a deep coastal current identified by Wanninkhof et al. (2015), which originates north of the MAB and has high DIC due to remineralization and a lack of ventilation to the atmosphere. The high pH and Ω_{arag} Gulf Stream influenced the carbonate system of MAB slope water to depths of ~100 m, and the deep coastal current caused lower pH and Ω_{arag} below 100 m in spring and fall. In summer, shelf break deep water was well-mixed with slope water, so it did not exhibit the same characteristic low pH and Ω_{arag} as in spring and fall.

4.1.3. Cold Pool Carbonate Chemistry Drivers

The MAB Cold Pool forms due to the onset of stratification in the spring and persists throughout summer (Castelao et al., 2008; Houghton et al., 1982; Z. Chen et al., 2018). Midshelf subsurface and deep water in the spring and summer exhibited lower than average Ω_{arag} and pH compared to the annual and seasonal means. These anomalies align with a general understanding of Cold Pool persistence, which indicates that strong seasonal stratification causes reduced ventilation of the Cold Pool to the atmosphere, therefore accumulating CO_2 from respiration, which decreases pH and Ω_{arag}. A complementary mechanism of Cold Pool persistence is the intrusion

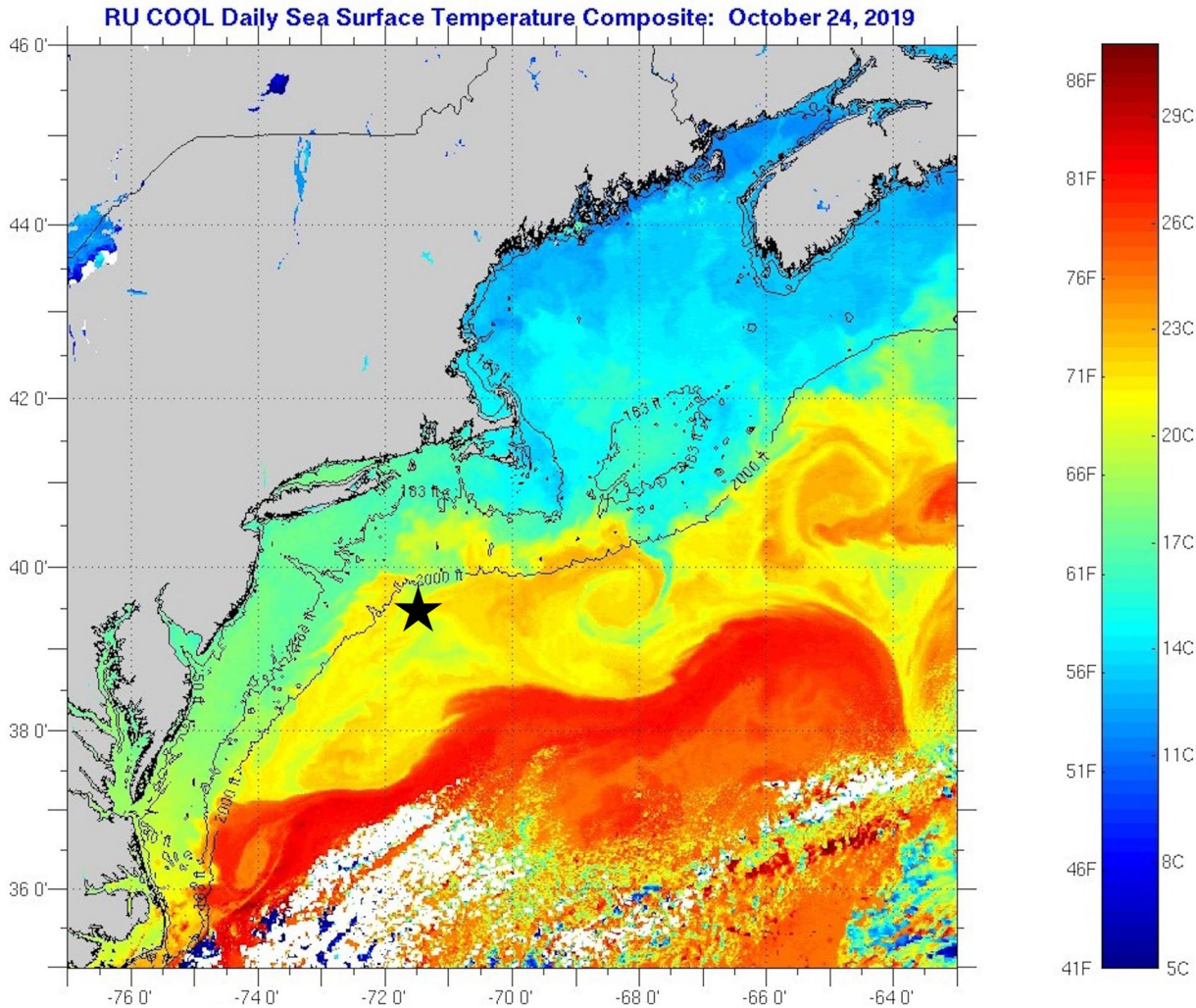

Figure 10. Mid-Atlantic Sea surface temperature observations on 24 October 2019 (fall glider deployment). Glider data showed an intrusion of Gulf Stream-influenced water onto the shelf, which was linked to high Ω_{arag} and pH. Glider location on 24 October is marked with a star. Map credit: Rutgers Coastal Ocean Observation Lab (https://marine.rutgers.edu/cool/sat_data/).

of water from north of the MAB, primarily the Georges Bank and the Gulf of Maine regions (originating from as far north as the Labrador Sea) (Brown et al., 2019; Castelao et al., 2008; Z. Chen et al., 2018). This source water has low Ω_{arag} compared with the MAB and therefore could be mixing into MAB shelf water and contributing to low Ω_{arag} and pH in Cold Pool subsurface water during summer.

Our analysis showed that water mass mixing drove low Ω_{arag} and pH in Cold Pool water relative to calculated annual and seasonal means. The importance of mixing is supported by both mechanisms of Cold Pool persistence, as it could indicate a lack of mixing between Cold Pool bottom water and the warmer surface layer or consistent along-isobath advection of more acidic northern water into the Cold Pool area. Further analysis of vertical mixing would provide insight into the interplay between stratification strength and horizontal water mass mixing as drivers of Cold Pool carbonate chemistry dynamics.

4.2. Decoupling of Ω_{arag} and pH Drivers

In the MAB, surface water Ω_{arag} and pH are driven by a combination of thermodynamics, air-sea gas exchange, and biological activity (Cai et al., 2020). In an open system, pH and Ω_{arag} experience two temperature-dependent responses, namely gas exchange and internal shifts in thermodynamic equilibrium due to changes in dissociation constants, K1 and K2. These two temperature-dependent responses counteract with each other in terms of their

effect on pH but enhance one another in terms of their effect on $[CO_3^{2-}]$, and as such, Ω_{arag} (Cai et al., 2020; Qi et al., 2020). In a closed system with no air-sea gas exchange, the opposite occurs, whereby pH is largely driven by temperature (cooling = higher pH), and Ω_{arag} is minimally affected by temperature. Though Cai et al. (2020) applied this concept to a spatial analysis of the carbonate system along a latitude gradient, the underlying principles can be applied to our seasonal data set.

The seasonal deployments showed little effect of gas exchange in winter, spring, and fall (Section 2.3), meaning they represent a closed system, while summer surface water is governed by the principles of an open system. Surface water had higher than average Ω_{arag} in summer and lower than average Ω_{arag} in winter, but lower pH in summer and higher pH in winter. This decoupling is expected in a closed system where pH is driven by seasonal temperature swings and Ω_{arag} is driven by faster, local processes such as photosynthesis, respiration, and local mixing events. Our driver analyses supported this, showing that surface Ω_{arag} in summer and winter was mainly driven by local mixing and biogeochemical activity, and winter surface pH was driven by temperature (Figure 7). However, in a deviation from the closed system ideal, summer surface pH was mainly driven by BGC and mixing.

The BGC influence on pH in summer likely reflects air-sea gas exchange that was identified as a contributing driver in summer surface water (Section 2.3). pH is more sensitive to changes in DIC caused by air-sea gas exchange than Ω_{arag} (Cai et al., 2021), which might explain why the influence of gas exchange was only reflected in pH. Additionally, the importance of mixing might reflect an overwhelming freshwater influence in surface water during the summer deployment (Section 4.1).

Because the glider data set covers only one deployment in each season, it is not possible to account for interannual differences in the importance of temperature here. Continued high-resolution monitoring of seasonal changes in the carbonate system will allow for analysis of interannual change and development of a regional carbonate system climatology for the MAB that will better identify long-term trends.

4.3. Comparison of Results to Past Studies

The results from our sensitivity analysis align well with previous studies of carbonate system drivers focused in localized regions within the NES or single season and single depth studies in the MAB. Xu et al. (2017) investigated short-term changes in surface carbonate chemistry along the U.S. East Coast using data from the summer ECOA-1 cruise in 2015. Similar to the results presented here, they found that Ω_{arag} increased from shore to shelf, driven mainly by physical mixing of slope water, though biological activity could alter this pattern on a shorter time scale. Xu et al. (2020) investigated long-term change in surface Ω_{arag} along the U.S. East Coast and concluded that TA and DIC are the dominant controls of Ω_{arag} on an interannual and decadal scale. Rheuban et al. (2019) conducted a monthly discrete sampling program in Buzzard's Bay, off the coast of Massachusetts, to investigate the influence of fresh water and nutrient inputs on surface carbonate chemistry. Akin to our study and Xu et al. (2017), they concluded that freshwater input is a strong local driver of carbonate chemistry in the inner shelf. Rheuban et al. (2019) also observed an important biogeochemical influence, which was linked to eutrophication based on total nitrogen measurements. Similarly, Wang et al. (2016) sampled six stations in Wilkinson Bay (Gulf of Maine) at 10–50 m depth resolution and found that Ω_{arag} was most strongly driven by seasonal cycles of photosynthesis and respiration, though mixing of low salinity water did impact Ω_{arag} in the nearshore. Common observations in past studies and the present study emphasize the importance of local processes of daily, seasonal, interannual, and decadal timescales on controlling the coastal carbonate system.

Glider data allowed the identification of important local controls on the carbonate system in higher spatial resolution than previous studies. Drivers were resolved at <1 m in depth and <1 km in distance over four seasons. This allowed the clear differentiation of carbonate parameters and their driving forces in surface and subsurface waters across the entire coastal shelf. The seasonal extent of acidified subsurface water in the MAB is necessary to understand in high resolution due to its importance to economically important fin- and shellfisheries.

In addition to providing high-resolution data, gliders have the unique ability to observe in areas that are difficult to access in discrete sampling programs, such as the continental shelf break. Cross-shelf glider deployments revealed the changing seasonal extent of Gulf Stream-influenced slope water intrusions onto the shelf, which mitigated acidified conditions based on its presence. Continued tracking of Gulf Stream intrusions, and colocating the physical and chemical variables with biological observations in future efforts, will allow a better understanding of ecological impacts of acidification for organisms inhabiting the shelf break.

Furthermore, glider missions provide continuous data streams that can show how short-term changes in environmental conditions change the system. For example, heavy rainfall during the summer deployment was linked to short-term decreases in surface pH in summer (Section 4.1.1), which may not have been captured with discrete sampling. While past studies have identified depth- and distance-related carbonate system changes, they have not been able to clarify the extent of driving forces at the fine scale allowed by glider technology.

5. Conclusions

This study decomposed the drivers of the carbonate system in the MAB in high resolution, spatially and temporally. High-resolution data were used to identify areas of the shelf and times of year that are most susceptible to acidification in the MAB. Sensitivity of Ω_{arag} and pH to water mass mixing, biogeochemical activity, temperature, and salinity varied over a spatial dimension in each season as well as between seasons compared to an annual mean. Water mass mixing and biogeochemical changes were consistently major drivers of change in the carbonate system, while seasonal temperature changes caused further deviation. Given these major drivers, future studies should focus on projected changes in freshwater runoff/precipitation in the nearshore and high salinity intrusions at the shelf break potentially linked to long-term changes in NAO and Atlantic Meridional Overturning Circulation. These processes may cause opposing acidification regimes in the nearshore and at the shelf break, with implications for the ecology of the region.

The sensitivity values derived here define how ocean properties determine the carbonate system, which can be used to improve coastal biogeochemical forecast models. These deployments cover one instance of each season, serving as a base understanding of seasonal carbonate system changes in the MAB. Continued seasonal monitoring will allow the derivation of a carbonate system climatology for the region and further investigation of interannual variability in dynamic carbonate system drivers like high salinity intrusions. Continued monitoring may also capture dynamic events not seen in the deployments analyzed here, like upwelling of cold and low-Ω_{arag} water due to seasonal wind shifts. This information will be valuable in fine-tuning habitat suitability studies and designing environmentally relevant laboratory experiments investigating the impact of acidification on commercially important species susceptible to acidification.

Data Availability Statement

Data supporting the conclusions made in this paper can be obtained online at http://slocum-data.marine.rutgers.edu/erddap/search/index.html?page=1%26itemsPerPage=1000%26searchFor=ru30.

Acknowledgments
The authors thank the Rutgers University Center for Ocean Observing Leadership (RUCOOL) faculty for facility support. The authors thank RUCOOL glider and software technicians (David Aragon, Nicole Waite, Chip Haldeman, Laura Nazzaro, and John Kerfoot) for their efforts in glider preparation, logistics, fieldwork, and mission piloting. The authors thank our colleagues at Sea-Bird Scientific (Andrew Barnard, Cristina Orrico, Charles Branham, Dave Murphy, Vlad Simontov, and Dave Walter) as well as colleagues at the Teledyne Webb Research (Clayton Jones, Clara Hulburt, and Christopher DeCollibus) for their technical expertise and collaboration. The authors thank Joe Salisbury and Travis Miles for their guidance and expertise in complex coastal oceanographic principles. Glider development, deployments, and carbonate chemistry laboratory work were funded by the National Science Foundation's Ocean Technology and Interdisciplinary Coordination program (National Science Foundation OCE1634520 and OCE1634582). E.W.F. received support from the Rutgers University School of Environmental and Biological Sciences Excellence Fellowship. This publication is the result of work sponsored by New jersey Sea Grant with funds from the National Oceanic and Atmospheric Administration (NOAA) Office of Sea Grant, U.S. Department of Commerce, under NOAA Grant #NA18OAR4170087 and the New Jersey Sea Grant Consortium. The statements, findings, conclusions, and recommendations are those of the authors and do not necessarily reflect the views of New Jersey Sea Grant or the U.S. Department of Commerce. NJSG-22-999.

References

Andres, M. (2016). On the recent destabilization of the Gulf Stream path downstream of Cape Hatteras. *Geophysical Research Letters*, *43*(18), 9836–9842. https://doi.org/10.1002/2016gl069966

Boehme, S. E., Sabine, C. L., & Reimers, C. E. (1998). CO_2 fluxes from a coastal transect: A time-series approach. *Marine Chemistry*, *63*(1–2), 49–67. https://doi.org/10.1016/s0304-4203(98)00050-4

Brodeur, J. R., Chen, B., Su, J., Xu, Y.-Y., Hussain, N., Scaboo, K. M., et al. (2019). Chesapeake Bay inorganic carbon: Spatial distribution and seasonal variability. *Frontiers in Marine Science*, *6*, 99. https://doi.org/10.3389/fmars.2019.00099

Brown, W., Schofield, O., Glenn, S., Kohut, J., & Boicourt, W. (2019). The Mid-Atlantic Bight Cold Pool, Part-1: Glider observations (SMAST Technical Report 19-0620).

Cai, W. J., Feely, R. A., Testa, J. M., Li, M., Evans, W., Alin, S. R., et al. (2021). Natural and anthropogenic drivers of acidification in large estuaries. *Annual Review of Marine Science*, *13*(1), 23–55. https://doi.org/10.1146/annurev-marine-010419-011004

Cai, W.-J., Hu, X., Huang, W.-J., Jiang, L.-Q., Wang, Y., Peng, T.-H., & Zhang, X. (2010). Alkalinity distribution in the western North Atlantic Ocean margins. *Journal of Geophysical Research*, *115*(C8), C08014. https://doi.org/10.1029/2009jc005482

Cai, W.-J., Hu, X., Huang, W.-J., Murrell, M. C., Lehrter, J. C., Lohrenz, S. E., et al. (2011). Acidification of subsurface coastal waters enhanced by eutrophication. *Nature Geoscience*, *4*(11), 766–770. https://doi.org/10.1038/ngeo1297

Cai, W.-J., Xu, Y. Y., Feely, R. A., Wanninkhof, R., Jonsson, B., Alin, S. R., et al. (2020). Controls on surface water carbonate chemistry along North American ocean margins. *Nature Communications*, *11*(1), 2691. https://doi.org/10.1038/s41467-020-16530-z

Carvalho, F., Kohut, J., Oliver, M. J., & Schofield, O. (2017). Defining the ecologically relevant mixed-layer depth for Antarctica's coastal seas. *Geophysical Research Letters*, *44*(1), 338–345. https://doi.org/10.1002/2016GL071205

Castelao, R., Glenn, S., Schofield, O., Chant, R., Wilkin, J., & Kohut, J. (2008). Seasonal evolution of hydrographic fields in the central Middle Atlantic Bight from glider observations. *Geophysical Research Letters*, *35*(3), L03617. https://doi.org/10.1029/2007gl032335

Chant, R. J., & Jurisa, J. T. (2013). Impact of offshore winds on a buoyant river plume system. *Journal of Physical Oceanography*, *43*(12), 2571–2587. https://doi.org/10.1175/jpo-d-12-0118.1

Chant, R. J., Wilkin, J., Zhang, W., Choi, B.-J., Hunter, E., Castelao, R., et al. (2008). Dispersal of the Hudson River plume in the New York Bight. *Oceanography*, *21*(4), 148–161. https://doi.org/10.5670/oceanog.2008.11

Chen, K., & He, R. (2010). Numerical investigation of the Middle Atlantic Bight shelfbreak frontal circulation using a high-resolution ocean hindcast model. *Journal of Physical Oceanography*, *40*(5), 949–964. https://doi.org/10.1175/2009jpo4262.1

Chen, K., He, R., Powell, B. S., Gawarkiewicz, G. G., Moore, A. M., & Arango, H. G. (2014). Data assimilative modeling investigation of Gulf Stream Warm Core Ring interaction with continental shelf and slope circulation. *Journal of Geophysical Research: Oceans*, *119*(9), 5968–5991. https://doi.org/10.1002/2014jc009898

Chen, Z., Curchitser, E., Chant, R., & Kang, D. (2018). Seasonal variability of the Cold Pool over the Mid-Atlantic Bight continental shelf. *Journal of Geophysical Research: Oceans*, *123*(11), 8203–8226. https://doi.org/10.1029/2018jc014148

DeGrandpre, M. D., Olbu, G. J., Beatty, C. M., & Hammar, T. R. (2002). Air-sea CO_2 fluxes on the US Middle Atlantic Bight. *Deep Sea Research*, *49*(20), 4355–4367. https://doi.org/10.1016/s0967-0645(02)00122-4

Dickson, A. (1990). Standard potential of the reaction: AgCl(s) + 1/2H_2(g) = Ag(s) + HCl(aq), and the standard acidity constant of the ion HSO_4^- in synthetic sea water from 273.15 to 318.15 K. *Journal of Chemical Thermodynamics*, *22*(2), 113–127. https://doi.org/10.1016/0021-9614(90)90074-z

Dickson, A., & Millero, F. J. (1987). A comparison of the equilibrium constants for the dissociation of carbonic acid in seawater media. *Deep-Sea Research*, *34*(10), 1733–1743. https://doi.org/10.1016/0198-0149(87)90021-5

Doney, S. C., Busch, D. S., Cooley, S. R., & Kroeker, K. J. (2020). The impacts of ocean acidification on marine ecosystems and reliant human communities. *Annual Review of Environment and Resources*, *13*(8), 83–112. https://doi.org/10.1146/annurev-environ-012320

Doney, S. C., Fabry, V. J., Feely, R. A., & Kleypas, J. A. (2009). Ocean Acidification: The other CO_2 problem. *Annual Review of Marine Science*, *1*, 169–192. https://doi.org/10.1146/annurev.marine.010908.163834

Fennel, K., Wilkin, J., Previdi, M., & Najjar, R. (2008). Denitrification effects on air-sea CO_2 flux in the coastal ocean: Simulations for the northwest North Atlantic. *Geophysical Research Letters*, *35*(24), L24608. https://doi.org/10.1029/2008gl036147

Fleming, N. (2016). *Seasonal and spatial variability in temperature, salinity, and circulation of the Middle Atlantic Bight* (PhD dissertation). Rutgers University.

Friis, K., Körtzinger, A., & Wallace, D. W. R. (2003). The salinity normalization of marine inorganic carbon chemistry data. *Geophysical Research Letters*, *30*(2), 1085. https://doi.org/10.1029/2002gl015898

Gledhill, D., White, M., Salisbury, J., Thomas, H., Misna, I., Liebman, M., et al. (2015). Ocean and coastal acidification off New England and Nova Scotia. *Oceanography*, *25*(2), 182–197. https://doi.org/10.5670/oceanog.2015.41

Gong, D., Kohut, J. T., & Glenn, S. M. (2010). Seasonal climatology of wind-driven circulation on the New Jersey Shelf. *Journal of Geophysical Research*, *115*(C4), C04006. https://doi.org/10.1029/2009jc005520

Grodsky, S. A., Reul, N., Chapron, B., Carton, J. A., & Bryan, F. O. (2017). Interannual surface salinity on Northwest Atlantic shelf. *Journal of Geophysical Research: Oceans*, *122*(5), 3638–3659. https://doi.org/10.1002/2016jc012580

Houghton, R. W., Shlitz, R., Beardsley, R. C., Butman, B., & Chamberlin, J. L. (1982). The Middle Atlantic Bight Cold Pool: Evolution of the temperature structure during summer 1979. *American Meteoroligcal Society*, *12*(10), 1019–1029. https://doi.org/10.1175/1520-0485(1982)012<1019:tmabcp>2.0.co;2

Hunt, C. W., Salisbury, J. E., Vandemark, D., Aßmann, S., Fietzek, P., Melrose, C., et al. (2021). Variability of USA East Coast surface total alkalinity distributions revealed by automated instrument measurements. *Marine Chemistry*, *232*, 103960. https://doi.org/10.1016/j.marchem.2021.103960

IPCC. (2019). Summary for policymakers. IPCC Special Report on the Ocean and Cryosphere in a Changing Climate.

Jiang, Z.-P., Tyrrell, T., Hydes, D. J., Dai, M., & Hartman, S. E. (2014). Variability of alkalinity and the alkalinity-salinity relationship in the tropical and subtropical surface ocean. *Global Biogeochemical Cycles*, *28*(7), 729–742. https://doi.org/10.1002/2013gb004678

Kroeker, K. J., Kordas, R. L., Crim, R., Hendriks, I. E., Ramajo, L., Singh, G. S., et al. (2013). Impacts of ocean acidification on marine organisms: Quantifying sensitivities and interaction with warming. *Global Change Biology*, *19*(6), 1884–1896. https://doi.org/10.1111/gcb.12179

Kwiatkowski, L., & Orr, J. C. (2018). Diverging seasonal extremes for ocean acidification during the twenty-first century. *Nature Climate Change*, *8*(2), 141–145. https://doi.org/10.1038/s41558-017-0054-0

Lewis, E., Wallace, D. W. R., & Allison, L. J. (1998). Program developed for CO_2 system calculations. https://doi.org/10.2172/639712

Linder, C. A., & Gawarkiewicz, G. (1998). A climatology of the shelfbreak front in the Middle Atlantic Bight. *Journal of Geophysical Research*, *103*(C9), 18405–18423. https://doi.org/10.1029/98jc01438

Manning, J. (1991). Middle Atlantic Bight salinity: Interannual variability. *Continental Shelf Research*, *11*(2), 123–137. https://doi.org/10.1016/0278-4343(91)90058-e

Mehrbach, C., Culberson, C. H., Hawley, J. E., & Pytkowicz, R. M. (1973). Measurement of the apparent dissociation constants of carbonic acid in seawater at atmospheric pressure. *Limnology & Oceanography*, *18*(6), 897–907. https://doi.org/10.4319/lo.1973.18.6.0897

Orr, J. C., Epitalon, J.-M., Dickson, A. G., & Gattuso, J.-P. (2018). Routine uncertainty propagation for the marine carbon dioxide system. *Marine Chemistry*, *207*, 84–107. https://doi.org/10.1016/j.marchem.2018.10.006

Orr, J. C., Fabry, V. J., Aumont, O., Bopp, L., Doney, S. C., Feely, R. A., et al. (2005). Anthropogenic ocean acidification over the twenty-first century and its impact on calcifying organisms. *Nature*, *437*(7059), 681–686. https://doi.org/10.1038/nature04095

Perez, F. F., & Fraga, F. (1987). Association constant of fluoride and hydrogen ions in seawater. *Marine Chemistry*, *21*(2), 161–168. https://doi.org/10.1016/0304-4203(87)90036-3

Qi, D., Chen, B., Chen, L., Lin, H., Gao, Z., Sun, H., et al. (2020). Coastal acidification induced by biogeochemical processes driven by sea-ice melt in the western Arctic ocean. *Polar Science*, *23*, 100504. https://doi.org/10.1016/j.polar.2020.100504

Rheuban, J. E., Doney, S. C., McCorkle, D. C., & Jakuba, R. W. (2019). Quantifying the effects of nutrient enrichment and freshwater mixing on coastal ocean acidification. *Journal of Geophysical Research: Oceans*, *124*(12), 9085–9100. https://doi.org/10.1029/2019jc015556

Richaud, B., Kwon, Y.-O., Joyce, T. M., Fratantoni, P. S., & Lentz, S. J. (2016). Surface and bottom temperature and salinity climatology along the continental shelf off the Canadian and U.S. East Coasts. *Continental Shelf Research*, *124*, 165–181. https://doi.org/10.1016/j.csr.2016.06.005

Runcie, J. W., Krause, C., Torres Gabarda, S. A., & Byrne, M. (2018). Technical note: Continuous fluorescence-based monitoring of seawater pH in situ. *Biogeosciences*, *15*(13), 4291–4299. https://doi.org/10.5194/bg-15-4291-2018

Saba, G. K., Goldsmith, K. A., Cooley, S. R., Grosse, D., Meseck, S. L., Miller, A. W., et al. (2019). Recommended priorities for research on ecological impacts of ocean and coastal acidification in the U.S. Mid-Atlantic. *Estuarine, Coastal and Shelf Science*, *225*, 106188. https://doi.org/10.1016/j.ecss.2019.04.022

Saba, G. K., Wright-Fairbanks, E., Chen, B., Cai, W.-J., Barnard, A. H., Jones, C. P., et al. (2019). The development and validation of a profiling glider deep ISFET-based pH sensor for high resolution observations of coastal and ocean acidification. *Frontiers in Marine Science*, *6*, 664. https://doi.org/10.3389/fmars.2019.00664

Saba, V. S., Griffies, S. M., Anderson, W. G., Winton, M., Alexander, M. A., Delworth, T. L., et al. (2016). Enhanced warming of the Northwest Atlantic Ocean under climate change. *Journal of Geophysical Research: Oceans*, *121*(1), 118–132. https://doi.org/10.1002/2015jc011346

Salisbury, J., & Jonsson, B. F. (2018). Rapid warming and salinity changes in the Gulf of Maine alter surface ocean carbonate parameters and hide ocean acidification. *Biogeochemistry*, *141*(3), 401–418. https://doi.org/10.1007/s10533-018-0505-3

Seitzinger, S. P. (1988). Denitrification in freshwater and coastal marine ecosystems: Ecological and geochemical significance. *Limnology & Oceanography*, *33*(4, part 2), 702–724. https://doi.org/10.4319/lo.1988.33.4part2.0702

Seitzinger, S. P., & Giblin, A. E. (1996). Estimating denitrification in North Atlantic continental shelf sediments. *Biogeochemistry*, *35*(1), 235–260. https://doi.org/10.1007/bf02179829

Sharp, J. D., & Byrne, R. H. (2020). Interpreting measurements of total alkalinity in marine and estuarine waters in the presence of proton-binding organic matter. *Deep Sea Research Part I: Oceanographic Research Papers*, *165*, 103338. https://doi.org/10.1016/j.dsr.2020.103338

Sharp, J. D., Pierrot, D., Humphreys, M. P., Epitalon, J.-M., Orr, J. C., Lewis, E. R., & Wallace, D. W. R. (2020). CO2SYSv3 for MATLAB (Version v3.0). Zenodo. http://doi.org/10.5281/zenodo.3950562

Siedlecki, S. A., Pilcher, D., Howard, E. M., Deutsch, C., MacCready, P., Norton, E. L., et al. (2021). Coastal processes modify projections of some climate-driven stressors in the California Current System. *Biogeosciences*, *18*(9), 2871–2890. https://doi.org/10.5194/bg-18-2871-2021

Siedlecki, S. A., Salisbury, J., Gledhill, D. K., Bastidas, C., Meseck, S., McGarry, K., et al. (2021). Projecting ocean acidification impacts for the Gulf of Maine to 2050. *Elementa: Science of the Anthropocene*, *9*(1), 00062. https://doi.org/10.1525/elementa.2020.00062

Song, S., Wang, Z. A., Gonneea, M. E., Kroeger, K. D., Chu, S. N., Li, D., & Liang, H. (2020). An important biogeochemical link between organic and inorganic carbon cycling: Effects of organic alkalinity on carbonate chemistry in coastal waters influenced by intertidal salt marshes. *Geochimica et Cosmochimica Acta*, *275*, 123–139. https://doi.org/10.1016/j.gca.2020.02.013

Sutton, A. J., Sabine, C. L., Feely, R. A., Cai, W.-J., Cronin, M. F., McPhaden, M. J., et al. (2016). Using present-day observations to detect when anthropogenic change forces surface ocean carbonate chemistry outside preindustrial bounds. *Biogeosciences*, *13*(17), 5065–5083. https://doi.org/10.5194/bg-13-5065-2016

Uppstrom, L. (1974). The boron/chlorinity ratio of deep-sea water from the Pacific Ocean. *Deep-Sea Research*, *21*(2), 161–162. https://doi.org/10.1016/0011-7471(74)90074-6

van Heuven, S., Pierrot, D., Rae, J. W. B., Lewis, E., & Wallace, D. W. R. (2011). *MATLAB program developed for CO_2 system calculations* (ORNL/CDIAC-105b). Carbon Dioxide Information Analysis Center, Oak Ridge National Laboratory, U.S. Department of Energy. https://doi.org/10.3334/CDIAC/otg.CO2SYS_MATLAB_v1.1

Wang, H. (2021). *Impact of canyon upwelling and downwelling in the Mid-Atlantic Bight* (PhD dissertation). The College of William & Mary.

Wang, Z., Lawson, G. L., Pilskain, C. H., & Maas, A. E. (2016). Seasonal controls of aragonite saturation state in the Gulf of Maine. *Journal of Geophysical Research: Oceans*, *122*(1), 372–389. https://doi.org/10.1002/2016JC012373

Wang, Z., Wanninkhof, R., Cai, W.-J., Byrne, R. H., Hu, X., Peng, T.-H., & Huang, W.-J. (2013). The marine inorganic carbon system along the Gulf of Mexico and Atlantic coasts of the United States: Insights from a transregional coastal carbon study. *Limnology & Oceanography*, *58*(1), 325–342. https://doi.org/10.4319/lo.2013.58.1.0325

Wanninkhof, R. (1992). Relationship between wind speed and gas exchange over the ocean. *Journal of Geophysical Research*, *97*(C5), 7373–7382. https://doi.org/10.1029/92jc00188

Wanninkhof, R., Barbero, L., Byrne, R., Cai, W.-J., Huang, W.-J., Zhang, J.-Z., et al. (2015). Ocean acidification along the Gulf Coast and East Coast of the USA. *Continental Shelf Research*, *98*, 54–71. https://doi.org/10.1016/j.csr.2015.02.008

Whitney, M. M. (2010). A study on river discharge and salinity variability in the Middle Atlantic Bight and Long Island Sound. *Continental Shelf Research*, *30*(3–4), 305–318. https://doi.org/10.1016/j.csr.2009.11.011

Wootton, J. T., Pfister, C. A., & Forester, J. D. (2008). Dynamic patterns and ecological impacts of declining ocean pH in a high-resolution multi-year dataset. *Proceedings of the National Academy of Sciences of the United States of America*, *105*(48), 18848–18853. https://doi.org/10.1073/pnas.0810079105

Wright-Fairbanks, E. K., Miles, T. N., Cai, W. J., Chen, B., & Saba, G. K. (2020). Autonomous observation of seasonal carbonate chemistry dynamics in the Mid-Atlantic Bight. *Journal of Geophysical Research: Oceans*, *125*(11), e2020JC016505. https://doi.org/10.1029/2020jc016505

Xu, Y. Y., Cai, W.-J., Gao, Y., Wanninkhof, R., Salisbury, J., Chen, B., et al. (2017). Short-term variability of aragonite saturation state in the central Mid-Atlantic Bight. *Journal of Geophysical Research: Oceans*, *122*(5), 4274–4290. https://doi.org/10.1002/2017JC012901

Xu, Y. Y., Cai, W.-J., Wanninkhof, R., Salisbury, J., Reimer, J., & Chen, B. (2020). Long-term changes of carbonate chemistry variables along the north American East Coast. *Journal of Geophysical Research: Oceans*, *125*(7), e2019JC015982. https://doi.org/10.1029/2019jc015982

Zeebe, R. E., & Wolf-Gladrow, D. A. (2001). *CO_2 in seawater: Equilibrium, kinetics, isotopes* (pp. 1–84). Elsevier.